Effect of nanostructured ferrites MFe_2O_4 (M= Cu, Co, Mg, Zn) on the thermal decomposition of ammonium nitrate

A.F. Cabrera , C.E. Rodríguez Torres , L.C. Juncal , M. Meyer , S.J. Stewart

PII: S2666-352X(21)00004-2
DOI: https://doi.org/10.1016/j.jaecs.2021.100026
Reference: JAECS 100026

To appear in: *Applications in Energy and Combustion Science*

Received date: 28 January 2021
Revised date: 31 March 2021
Accepted date: 12 April 2021

Please cite this article as: A.F. Cabrera , C.E. Rodríguez Torres , L.C. Juncal , M. Meyer , S.J. Stewart , Effect of nanostructured ferrites MFe_2O_4 (M= Cu, Co, Mg, Zn) on the thermal decomposition of ammonium nitrate, *Applications in Energy and Combustion Science* (2021), doi: https://doi.org/10.1016/j.jaecs.2021.100026

Highlights

- Nanostructured MFe_2O_4 act as catalysts in the decomposition of ammoniun nitrate
- The addition of MFe_2O_4 reduces the onset temperature of the exothermic reaction of NH_4NO_3.
- The metal cations of ferrites act as acidic Lewis sites removing ammonia.
- The catalytic performance is associated with the electronegativity of M^{2+} cations.
- The best catalytic performance is achieved with the addition of $CoFe_2O_4$

Effect of nanostructured ferrites MFe_2O_4 (M= Cu, Co, Mg, Zn) on the thermal decomposition of ammonium nitrate

A. F. Cabrera, C. E. Rodríguez Torres, L. C. Juncal, M. Meyer and S. J. Stewart*

IFLP-CCT-La Plata-CONICET and Departamento de Física, Facultad de Ciencias Exactas, Universidad Nacional de La Plata, C. C. 67, 1900 La Plata, Argentina

Abstract

Ammonium nitrate (NH_4NO_3) represents a cheap, chlorine-free alternative to ammonium perchlorate for use as an oxidant for solid propellants. But its poor ignitability and low burning rate are all disadvantages to achieve such purposes. For this reason, it is necessary to carry out studies to improve its combustion characteristics, seeking to combine it with catalysts or fuels. The present work explores the possibility of improving its combustion characteristics by adding ferrites as catalysts. Nanostructured ferrites MFe_2O_4 (M= Mg, Co, Cu, and Zn) synthesized by autocombustion method were tested as catalysts for the thermal decomposition reaction of ammonium nitrate under open, partially open or sealed conditions. The ferrites were characterized by XRD, SEM, UV-vis spectrophotometry and Mössbauer spectroscopy. All the MFe_2O_4 samples are single phased with a cubic spinel structure and average sizes, *L*, ranging from about 9 ($CoFe_2O_4$) to 25 nm ($CuFe_2O_4$). The catalytic effect of MFe_2O_4 on the thermal decomposition of NH_4NO_3 was investigated by thermogravimetric analysis and differential scanning calorimetry techniques. The process was also followed in a volumetric Sieverts type apparatus. The results indicate that only under sealed conditions the addition of these ferrites has influence in the decomposition process of AN. The incorporation of any of these ferrites decreases the onset temperature of the process manifested itself through an exothermic reaction, and also increases the amount of heat released in the reaction. The Co-ferrite showed the best efficiency causing the onset temperature to drop around 60 ºC. The catalytic performance is correlated with the electronegativity of M^{2+} cations, which act as Lewis acid sites that interact with the gas molecules.

Graphical abstract XX

Keywords: ammonium nitrate, solid propellants, spinel ferrites, nanoparticle catalysts

Corresponding author: stewart@fisica.unlp.edu.ar

1. Introduction

Solid propellants are mainly used in rocket propulsion applications [1] and also for fracturing wells in borehole mining [2,3]. They are very energetic and produce high temperature gaseous products by combustion. A high material density of solid propellants leads to a high energy density needed for producing the required propulsive or fracturing force. A solid propellant consists of several chemical ingredients such as oxidizer, fuel, binder, plasticizer, curing agent, stabilizer, and cross-linking agent. Different chemical ingredients and their proportions result in different physical and chemical properties, combustion characteristics, and performance [4]. Most solid propellants employ ammonium perchlorate (AP) as the main oxidizer due to its high performance and good burning rate. However, one of the preliminary products of AP combustion is HCl, which in the presence of water forms hydrochloric acid, which in turn produces smoke and is highly toxic. To avoid these environmental problems clean burning propellants such as ammonium nitrate (NH_4NO_3, AN) are being tested [5,6]. AN is a synthetic salt widely used in the chemical industry and in agriculture [1,7-9]. It has a wide application in the area of nitrogen fertilizers, since it acts as a source of ammonia and nitrate ions vital to plants [9]. The products from its decomposition (100% gaseous) are chlorine free and smokeless; it has a positive oxygen balance and presents high stability in the lower temperature range [1,5,7]. Besides, it is one of the cheapest and easily available compounds. However, its use in the field of solid propellants is rather limited due to its poor ignitability, low energy, low burning rate under low-pressure conditions and hygroscopicity. Then, it is necessary to carry out studies to improve the combustion characteristics of AN. Several studies have been conducted in this sense seeking to combine it with catalysts or fuels [5,7,10].

Transition metal oxides (TMO) nanoparticles have been proved to be effective additives to increase the burning rate and ignitability of AN propellants as well as to modify the onset temperature and the energy of activation of the AN decomposition [11-15]. Mostly, the TMO effects on AN decomposition have been tested using catalysts having one or two metal ions occupying a unique metal site. It has been found that the catalytic effect of TMO is attributed to several reasons such as their semiconductor properties (degree of *p* or *n* nature), to the activation of proton or electron transfer processes, to the role of metal ions in the reduction processes, amongst others [11-14]. But the actual mechanism of activity is still not known to any certainty. Among TMO, ferrite compounds (MFe_2O_4, where M is a metallic divalent ion) have largely been studied because their physical and physico-chemical properties are tunable by changing the accommodation of cations between the two available metallic sites of their spinel structure (of octahedral or tetrahedral symmetry). The catalytic performance of ferrites for many reactions depends on the redox properties of a particular metal ion and on the way the active sites distribute among the surface spinel sites [16,17]. While several studies have been focused on the catalytic effect of nanoferrites on the thermal decomposition of AP [18,19], only a few reported its performance on the

AN decomposition [12,14]. For example, Xu et al. [12] found that $CuFe_2O_4$ and $CuFe_2O_4$/graphene oxide with Fe_2O_3 distributed on the surface of the ferrites have catalytic effects on the thermal decomposition of AN (the initial and maximum temperatures of the decomposition reaction change to lower values and the energy of activation decreases). Vara et al. [14] applied thermogravimetric techniques to investigate the effect of mixed CuNi, CoMn and NiZn ferrites prepared by coprecipitation as catalysts for the thermal behavior of AN and solid propellants based on AN. They also found that the addition of these ferrites reduces the activation energy and the decomposition temperature of AN, with CoMn being the ferrite that shows the best catalytic performance.

In this work, we explore the improvement of the combustion characteristics of ammonium nitrate by adding MFe_2O_4 nanostructures (M= Mg, Co, Cu and Zn) obtained by autocombustion. The nanoferrites were characterized by XRD, SEM, UV-vis and Mössbauer spectroscopies. The effect of the catalysts on the AN decomposition were investigated by using thermogravimetric, differential scanning calorimetry techniques and also using a volumetric Sieverts type apparatus where temperature and pressure can be monitored simultaneously along the thermal treatment. Here we will show that the addition of nanoferrite decreases the onset temperature of the decomposition and moreover, under closed condition the reaction changes from endothermic to exothermic type. The latter could be useful for combustion when the oxidizer is combined with fuel.

2. Experimental

2. 1. Sample fabrication

Nanostructured MFe_2O_4 ferrites (M= Mg, Co, Cu, and Zn) were obtained by the autocombustion method [20]. High purity metal nitrates $M(NO_3)_2.6H_2O$ (M: Mg, Co, Cu, Zn), $Fe(NO_3)_3.9H_2O$ and citric acid, $C_6O_7H_8$, were mixed in stoichiometric amounts required for the chemical reaction:

$$M(NO_3)_2 + 2Fe(NO_3)_3 + \frac{20}{9}C_6O_7H_8 \rightarrow MFe_2O_4 + \frac{80}{9}H_2O + \frac{40}{3}CO_2 + 4N_2 \qquad (1)$$

Each mixture was heated on a hot-plate under continuous stirring until gelification occurs. Then, the gel was kept at 80 ºC until the combustion took place. The obtained powders were thermally treated at 200 °C for two hours. The as-prepared Mg, Co, Cu and Zn-ferrite samples are labeled MgFO, CoFO, CuFO and ZnFO, respectively. The purity of all the obtained samples was verified by the XRD results (see Section 3.1), which only show the characteristic of the spinel structure of the ferrite.

2. 2. Ferrite characterization

X-ray diffraction (XRD) data of MgFO, CoFO, CuFO and ZnFO were recorded using a Philips PW 1710 diffractometer (Cu-Kα, λ=1.5406 Å). The full width at half maximum (FWHM) of the most intense (311) Bragg line was used to estimate the average crystallite size (*L*) through the Debye-Scherrer formula

$$L = \frac{k\lambda}{FWHM\ cos\theta} \qquad (2)$$

with k=0.9 and θ is the angle corresponding to the 2θ position of the peak. The *L* results are shown in Table I.

The samples were morphologically characterized with scanning electron microscopy (SEM, FEI ESEM Quanta 200). Room temperature ^{57}Fe Mössbauer spectra of MgFO, CoFO, CuFO and ZnFO were taken in transmission geometry with a nominal 50 mCi ^{57}Co/Rh source with a linear velocity waveform. Isomer shifts (IS) are referred to α-Fe. The diffuse reflectance measurements were taken with a Shimadzu UV-2600 spectrometer with IRS-2600Plus attachment.

2. 3. TGA and DSC thermal analysis

The thermal decomposition of AN and AN+MFe_2O_4 was analyzed using a Differential Scanning Calorimeter Shimadzu (DSC-50) and a Thermogravimetric Analyzer Shimadzu (TGA-50H). Mixtures AN+MFe_2O_4 were prepared using a 95:5 AN:MFe_2O_4 mass ratio and mixed in an agate mortar. This ratio was selected considering previous studies about the effect of salts and oxides on the AN decomposition (see, for instance, Refs. [12,14,21,22]). The DSC measurements were performed placing the samples in an aluminum crucible while a platinum crucible was used for thermogravimetric assays (TGA) (sample weight around 200 mg) along a temperature range 25-500°C with a heating rate of 10°C/min and under nitrogen atmosphere (20 ml/min). Three different crucibles were used in calorimetric measurements: i) open pan, ii) pan with a lid and iii) sealed pan, which we describe as open, partially open and sealed conditions, respectively (see Supplementary Information, S. I.).

2. 4. Experimental details of the treatments performed in a reactor

Sieverts type apparatus was used to carry out the thermal treatments in a closed reactor (see S. I.). A standard known volume was used to determine the effective reactor volume at the working temperature. The instantaneous pressure as a function of time $P(t)$ was measured with a gauge transducer sensor and the temperature as a function of time $T(t)$ was measured with a PT 100 sensor in contact with the sample, inside the reactor. Typically, values of $P(t)$ and $T(t)$ were taken each second. Amounts of 100–200 mg of AN or AN-ferrite

mixtures were placed in the sample holder, which consists of a stainless-steel cylinder of about 0.6 cm^3. A quartz wool filter was placed at the ends of the sample holder to keep the powder inside.

3. Results

3. 1. Results of the catalysts characterization

The XRD patterns of samples MFe_2O_4 (M= Mg, Co, Cu, Zn) only show broad diffraction lines belonging to the cubic spinel structure (Fig. 1). The lattice parameter (*a*) and the average crystallite sizes (*L*) are shown in Table I. The *a* values are not far from those reported for the corresponding bulk spinel ferrites (Table I) [23]. The *L* value for Cu-ferrite almost duplicates the *L* sizes estimated for MgFO and ZnFO. The CoFO sample presents the lowest crystallite size (around 9 nm).

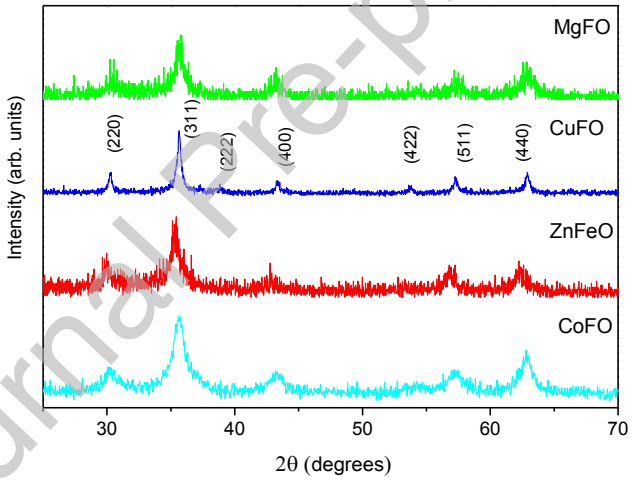

Figure 1: XRD diffractograms of M- ferrites obtained by autocombustion. Miller indices (*hkl*) indicate the spinel characteristic lines

Figure 2 shows SEM micrographs of the synthesized ferrites. In all cases, the samples present irregular shapes with cavities or holes of different sizes probably formed due to the release of gases during the combustion process. The surface of ZnFO particles shows relatively large smooth regions in comparison with the other ferrites, while MgFO presents a higher density of smaller cavities.

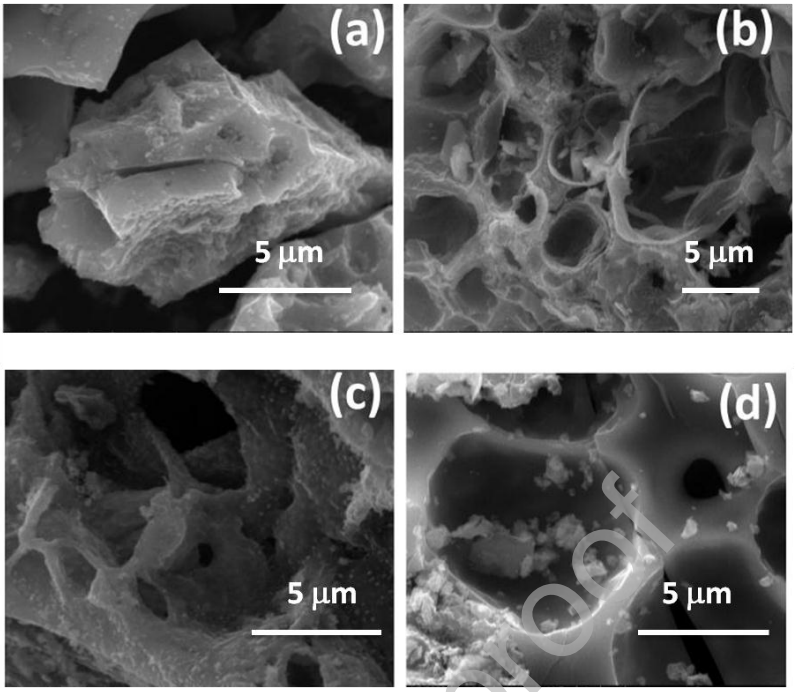

Figure 2: SEM micrographs corresponding to (a) MgFO, (b) CoFO, (c) CuFO and (d) ZnFO ferrites samples.

Sample	***L*** **(nm)**	***a*** **(Å)**	**Reported *a*** **(Å)**	T_c **(K)**	**Reported** T_c **(K)**	E_g **(eV)**
MgFO	12.2_1	8.355_2	8.36	720_{10}	713	2.22_4
CuFO	25.0_2	8.377_1	8.37*	770_{10}	780	2.02_3
ZnFO	11.2_1	8.362_2	8.44	665_{10}	11 (T_N)	2.19_4
CoFO	8.5_4	8.351_9	8.39✦		728	2.51_2

Table I: Average crystallite size (*L*) and lattice parameter (*a*) resulting from the XRD data and magnetic ordering temperature (T_C) determined by TGA measurements. The T_C of CoFO was not obtained. Values of reported *a* and T_C (or the Neel temperature T_N for ZnFO) of cubic ferrites are also included (Refs. [23,25]). (*PDF # 77-0010;✦PDF # 22-1086). E_g is the energy band gap estimated from the UV-Vis spectroscopy data.

To estimate the magnetic ordering temperature (T_C), thermogravimetric measurements were performed with an 8 mT permanent magnet placed at the bottom of the samples. The T_C values were determined from the mass-loss difference during TGA running with and without magnetic field (see Table I). The UV–vis diffuse reflectance spectra recorded for these samples (not shown) presented high reflectance in the visible range associated to the direct band absorption of these compounds. They have relatively narrow band gap energies E_g with values ranging from 2 to 2.5 eV (see Table I) [24].

The Mössbauer spectra of all ferrites (see S. I.) indicate that the iron atoms are in the 3+ oxidation state except for a small contribution from Fe^{2+} present in the spectra of CoFO and ZnFO (Table I of supplementary information lists the Mössbauer parameters). All spectra have superparamagnetic components due to the nanostructured character of the ferrites. Also, the spectra of CoFO, CuFO and MgFO present resolved magnetic field components whose hyperfine parameters indicate that iron ions occupy both octahedral and tetrahedral sites as expected for these inverted ferrites [23]. The spectrum of ZnFO only shows non-magnetic components that we assigned to paramagnetic and superparamagnetic (SPM) contributions (see S. I.). The presence of a SPM broad doublet and the T_C value above room temperature (Table I) indicate that this ferrite is partially inverted, as is usually the case when $ZnFe_2O_4$ is nanostructured [26].

3. 2. Experimental results of the thermal treatments of AN and AN+ MFe_2O_4

The performance of MgFO, CoFO, CuFO and ZnFO ferrites on the thermal decomposition of AN was investigated using TGA and DSC analysis. Firstly, we analyze the decomposition of pure AN under three different conditions for the DSC scans, i. e., by using i) an open pan, ii) a pan with a lid or ii) a sealed aluminum pan. These results are shown in Fig. 3. The DSC curves of pure AN present four endothermic peaks. Peaks labeled (1) and (2) (see Fig. 3 (a) and Table II) account for the structural phase transformations of AN, peak (3) corresponds to the melting of AN and peak (4) to its thermal decomposition [5,27]. The features of the first three DSC peaks remain, as expected, at the same temperatures under all conditions. However, the peak (4) that corresponds to an endothermic process under i) and ii) conditions, in the sealed case iii) the DSC results indicates that there is a superposition of exothermic and endothermic peaks. In addition, the temperature range in which the decomposition reaction takes place is also different, it occurs at higher temperatures under sealed conditions. The TGA curve (Fig. 3 (b)) shows that the weight loss during the decomposition is complete and occurs along the ranges of temperature: 180-250 ºC (open pan), 280-330 ºC (sealed pan). The temperature of the maximum change of TGA curve (minimum peak in DTG curve) coincides with the temperature of peak (4) of the DSC curve of condition i), i. e., when the pan is open during the TGA (Figs. 3(a) and 3(c)). On the contrary, when using a sealed pan there is a shift of around 30 ºC between the onset of DSC peak (see inset Fig 3 (c)) and the weight change in TGA and also evidenced in the DTG curve.

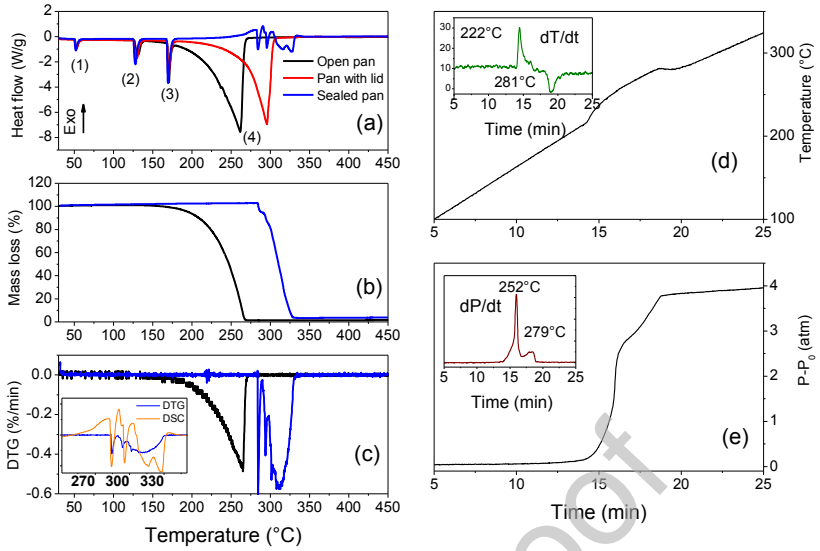

Figure 3: Thermal treatments for pure ammonium nitrate: (a) Differential scanning calorimetry (DSC) analysis under the three different conditions: open pan, pan with a lid and sealed pan, (b) Thermogravimetric analysis (TGA) curves for open and sealed pan conditions, (c) Differential thermogravimetric DTG curves for open and sealed pan conditions (inset: DTG and DSC curves for sealed pan), (d) Temperature of the reactor chamber and (e) change of pressure as a function of time. Insets of (d) and (e) show the corresponding derivatives.

The performance of MgFO, CoFO, CuFO and ZnFO ferrites on the thermal decomposition of AN was investigated using TGA and DSC analysis. Firstly, we analyze the decomposition of pure AN under three different conditions for the DSC scans, i. e., by using i) an open pan, ii) a pan with a lid or ii) a sealed aluminum pan. These results are shown in Fig. 3. The DSC curves of pure AN present four endothermic peaks. Peaks labeled (1) and (2) (see Fig. 3 (a) and Table II) account for the structural phase transformations of AN, peak (3) corresponds to the melting of AN and peak (4) to its thermal decomposition [5,27]. The features of the first three DSC peaks remain, as expected, at the same temperatures under all conditions. However, the peak (4) that corresponds to an endothermic process under i) and ii) conditions, in the sealed case iii) the DSC results indicates that there is a superposition of exothermic and endothermic peaks. In addition, the temperature range in which the decomposition reaction takes place is also different, it occurs at higher temperatures under sealed conditions. The TGA curve (Fig. 3 (b)) shows that the weight loss during the decomposition is complete and occurs along the ranges of temperature: 180-250 ºC (open pan), 280-330 ºC (sealed pan). The temperature of the maximum change of TGA curve (minimum peak in DTG curve) coincides with the temperature of peak (4) of the DSC curve of condition i), i. e., when the pan is open during

the TGA (Figs. 3(a) and 3(c)). On the contrary, when using a sealed pan there is a shift of around 30 ºC between the onset of DSC peak (see inset Fig 3 (c)) and the weight change in TGA and also evidenced in the DTG curve.

Condition	**Peak**	***T* onset (ºC)**	***T* peak (ºC)**	**Heat (J/g)**	**Identification[a]**
i) Open pan	(1)	50.3_5	52.9_5	-21_1	IV→ III
	(2)	126.5_5	131.1_5	-42_1	II →I
	(3)	168.7_5	170.3_5	-65_1	Melting
	(4)	209.4_5	261.7_5	-990_1	Decomposition
DTG		189_2	266_2		
ii) Pan with lid	(1)	49.5_5	52.6_5	-24_1	IV→ III
	(2)	125.0_5	130.1_5	-51_1	II → I
	(3)	168.4_5	170.3_5	-69_1	Melting
	(4)	255.1_5	295.6_5	-1000_1	Decomposition
iii) Sealed pan	(1)	50.2_5	52.1_5	-28_1	IV→ III
	(2)	125.4_5	128.0_5	-60_1	II → I
	(3)	168.0_5	169.6_5	-81_1	Melting
	(4)	240_2	246-262*	-23_1	Decomposition

Table II: Values corresponding to the DSC and TGA results on pure AN. [a]Refs. [5,7,28]. *Temperature range.

The decomposition process was also followed by the thermal treatment carried out in the reactor where pure AN was heated up to 400 ºC at a heating rate of 10 °C/min. Fig. 3 (d) shows that the increment of the chamber temperature with the time deviates from a linear trend when the temperature reaches 213 ºC after 15 minutes of heating. This is reflected in the derivative curve, dT/dt *vs.* time, shown in the inset of Fig. 3 (e). We observe that, in this case, the decomposition process is exothermic. During the process the reactor pressure increases about 4 atm (see Fig. 3 (e)). Further, the pressure increment occurs at different rates. This can be seen in the change of slope of $P(t)$ (Fig. 3(e) and inset Fig. 3 (e)). Its derivative dP/dt shows two maxima, at 252 ºC and 279 ºC. We observe that the AN

decomposition takes place along an interval of temperature, ΔT_D=48 ºC, taken as the difference between the temperatures at which the maximum (*dT*/*dt* max) and minimum (*dT*/*dt* min) of *dT*/*dt* take place (inset Fig. 3 (d)). It is worth mentioning that the maximum of *dP*/*dt* occurs at a temperature about 25 ºC higher than where the maximum of *dT*/*dt* is, indicating that the reaction products remain in liquid phase. This is in line with the delay observed between the exothermic reaction and the weight change in the DSC measurement when using the sealed pan.

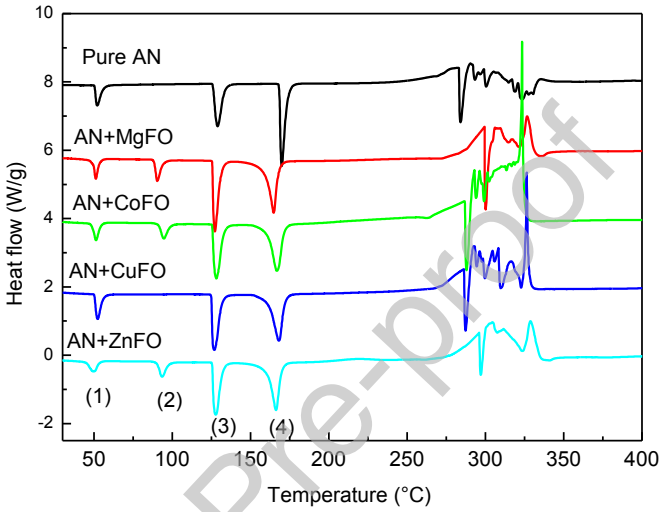

Figure 4: DSC curves for pure AN and AN+MFe_2O_4 mixtures placed in a sealed aluminum pan. The curves were shifted vertically for a better visualization.

No appreciable changes were observed in the TGA and DSC results corresponding to AN+MFe_2O_4 mixtures under condition i) in comparison with those obtained for pure AN (see Supplementary Information). However, under sealed condition iii) the addition of ferrites indeed changes on these results (Figs 4 and Table III). We observe that, except for AN+CuFO, with the addition of ferrites the DSC curves show the endothermic peak at about 86 ºC corresponding to the III→ II) transformation [5,7,28]. Furthermore, in all the mixtures the melting temperature (peak (3)) slightly shifts to lower values (Table III). Finally, the decomposition reaction becomes more exothermic with the aggregation of ferrites. The highest heat of the reaction corresponds to AN+CoFO while the lowest one was registered for AN+MgFO (Table III).

Fig. 5 shows the time evolution of temperature and pressure in the reactor chamber for AN and AN+MFe_2O_4 mixtures while the extremes values of the corresponding derivatives are plotted in Fig. 6. In all cases, the reaction is predominantly exothermic. We observe that

the onset of the reaction shifts to lower temperatures for all the AN+MFe_2O_4 samples (Figs. 5 and 6). The major temperature shift of around 60 ºC was registered for AN+CoFO, being the order from the highest to the lowest temperature shift as follows: CoFO > MgFO > CuFO > ZnFO. The temperature at which the maximum rate of change of $P(t)$ occurs is rather above the onset temperature and it decreases between 10 and 15 ºC with respect to pure AN, except for AN+MgFO in which there is a slight increase of about 5 ºC (Fig. 6). It is worth mentioning that, coincidentally with pure AN, the derivative of $P(t)$ shows in all the cases a second but less intense maximum (inset Fig. 3(e) and (S. I.)).

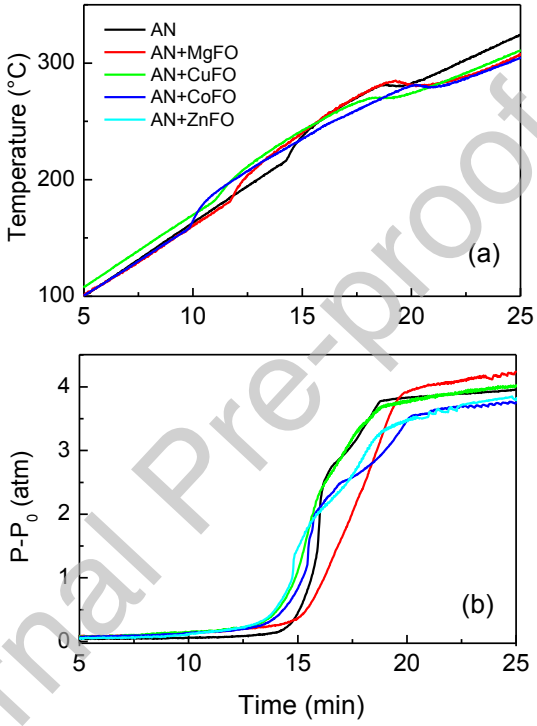

Figure 5: (a) Temperature of the reactor chamber and (b) change of pressure (P-P_0) and as a function of time for treatments of pure AN and AN+ferrite mixtures.

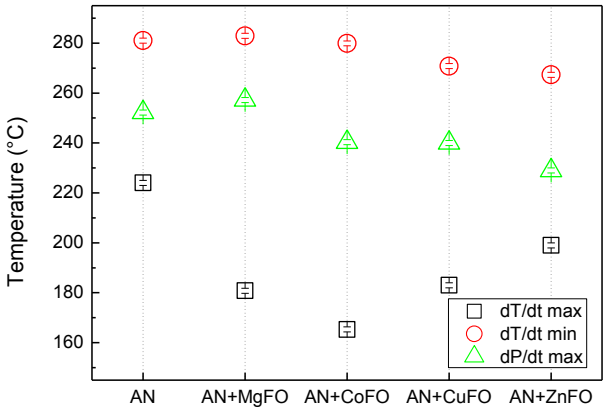

Figure 6: Graph showing the temperatures at which the maxima (*dT*/*dt* max) and minima (*dT*/*dt* min) of the derivatives of *T*(*t*) and of the maximum change of pressure *P*(*t*) are registered in the reactor for AN and AN+ferrite mixtures (Fig. 3). Error bars are included inside the symbols.

4. Discussion

4. 1 On the thermal decomposition of pure ammonium nitrate at different conditions

Previous studies on AN showed that this salt melts at 169 ºC and its decomposition initiates as soon as it melts [5,7,27,29,30]. The equilibrium in molten AN can be represented by the following reaction:

$$NH_4NO_3(l) \rightarrow NO_3^-(l) + NH_4^+(l) \rightleftarrows HNO_3(l) + NH_3(l) \qquad (3)$$

Thus, according to eq. (3) molten AN firstly dissociates into NO_3^- and NH_4^+ followed by a proton transfer process to produce HNO_3 and NH_3. In a second stage, HNO_3 and NH_3 undergo an endothermic vaporization (Eqs. (4) and (5)).

$$HNO_3(l) \rightleftarrows HNO_3(g) \qquad (4)$$

$$NH_3(l) \rightleftarrows NH_3(g) \qquad (5)$$

Further reactions occur since HNO_3 decomposes into diverse products ($NO_3^-, NO_2^+, H_2O, N_2O_5, H_3O^+, etc.$) and some of these products, in turn, are able to oxidize both NH_4^+ and NH_3. The reaction pathways and products formed strongly depend on whether the system is sealed, that is, if the reaction products build up and increase pressure, or they are allowed to escape (Ref.[27] and references therein].

Babrauskas et al. [27] reported that there is a competition between the endothermic decomposition into HNO_3 and NH_3 and the exothermic oxidation reactions, the equilibrium between them being sensitive to heating conditions. These authors found that if the reaction products are allowed to accumulate unrelieved during heating, an increasing pressure will be reached and a deflagration explosion will occur. But if the system is open and reaction products are allowed to escape, then steady-state conditions will be established and the system will reach a quasi-boiling point [Ref. 27 and references therein].

Our results concerning pure AN are in agreement with these previous observations. Indeed, our DSC studies performed in an open pan or in the pan with a lid show an endothermic reaction takes place above the AN melting point. However, under sealed conditions (DSC scans and treatment in the reactor) AN also undergoes an exothermic reaction. Furthermore, this exothermic process is more intense than the endothermic one, which suggests that relatively high pressures reduce the evaporation of HNO_3 and NH_3.

4. 2. AN+ MFe_2O_4: effects of nanoferrites as additives

Concerning the role of ferrites as catalysts in the decomposition of AN, we observe that their inclusion does not modify the process unless the heating was performed under a sealed condition. In such a case, the more relevant results are that the heat released measured by DSC experiments increases while the onset temperature of the exothermic reaction detected in the reactor decreases with respect to pure AN. Considering the heat released during the decomposition the order of the effect is: CoFO > CuFO > ZnFO > MgFO. Although the major modifications are observed for the ferrite with the smallest crystallite size (CoFO), there is no a direct correlation between activity and size as CuFO with almost twice the *L* value of ZnFO and MgFO shows a better performance than these two ferrites. Neither there is an influence of the morphology of the samples as they on the whole present a similar aspect. Thus, to interpret the AN+MFe_2O_4 results, other possibilities like concerning the role of metal oxides as catalysts need to be considered.

It is known that oxide metal cations act as acidic Lewis sites that can interact with Lewis bases forming a donor-acceptor bond. In the present case, the Lewis base could be the ammonia formed in the vaporization stage, which is known to act as an inhibitor of the thermal decomposition of AN [5]. The interaction between NH_3 and metallic sites has been extensively studied in the literature [31-35]. For instance, Tsyganenko et al. [31] in an infrared study of ammonia absorption on several transition metal oxide surfaces suggested that part of ammonia dissociates on the oxide surface with the formation of hydroxyl and NH_2 groups. Other results pointed out that Fe_2O_3 interacts with NH_3 according with the following reaction [12,33]:

$$Fe^{3+} + NH_3 \rightarrow Fe^{2+} + NH_2 + H^+ \qquad (6)$$

To explain the effect of CuO on the decrease of the activation energy for AN thermal decomposition Vargeese et al. [36] suggested that CuO nanorods added to AN provide Lewis acid or metal active sites for the removal of NH_3 through the adsorption of NH_3 and its subsequent conversion into N_2.

Cannon et al. [37] have remarked the important role played by metal cations and their electronic configurations in the catalytic performance of metal oxides in the decomposition of potassium chlorate. It has also been demonstrated that metal cations with high electronegativity are more effective to participate in the adsorption of gas molecules on the surface of a semiconductor oxide [34]. These results are indicative of the correlation that exists between the Lewis acid (or base) strength of metal oxides with the electronegativity of its metal element or ions. In the case of ferrite oxides, their effectiveness for catalytic applications resides in its cationic composition, the metal-oxygen strength and the distribution of cations in active sites at the surface particle, the latter mainly related to the spinel octahedral sites [16]. For instance, a previous study about the use of ferrites as catalysts for the benzoylation reaction [38] attributed their activity to the surface Lewis acid sites provided by the cations at surface octahedral spinel sites, where the intrinsic acidity has the Co > Ni> Cu-ferrite tendency.

Sample	***T* peak (peak 3) (ºC)**	**Realeased Heat (peak 4) (J/g)**		χ_i^*
Pure AN	169.2_5	-23_1		
AN+MgFO	164.8_5	130_1	Mg^{2+}	6.55
AN+CoFO	166.8_5	410_1	Co^{2+} Co^{3+} $Co^{2+/3+}$	9.4 13.16 11.3
AN+CuFO	168.1_5	240_1	Cu^{2+}	9.5
AN+ZnFO	166.2_5	220_1	Zn^{2+}	8.25
			Fe^{3+}	12.81

Table III: Temperature values of peak (3) and heat released corresponding to the decomposition reaction peak (4) extracted from DSC results of hermetically sealed condition measurements. $^*\chi_i$ is the electronegativity of metal ion in metal oxide supports (Ref. [40]).

Considering that the strong Lewis acidity of ferrites mainly originates in the presence of ferric ions (Table III) and that all these compounds contain Fe^{3+}, the different magnitude of

their effects on the AN thermal decomposition can be attributed to the kind of M^{2+} cations at surface sites. The octahedral sites of partially inverted $CoFe_2O_4$, $CuFe_2O_4$ and $MgFe_2O_4$ are occupied by both Fe^{3+} and M^{2+} cations (Cu^{2+}, Mg^{2+} or Co^{2+}) [23]. Although $ZnFe_2O_4$ in its bulk state is a normal spinel with only Fe^{3+} at octahedral sites, when it is nanostructured it becomes partially inverted with Zn^{2+} and Fe^{3+} distributed between the two spinel sites [26]. In addition, the cationic inversion, which is a defect in volumetric $ZnFe_2O_4$, becomes energetically favorable on the surface [39]. In our case, the partial inversion of ZnFO is suggested by the Mössbauer results and the detection of a magnetic ordering temperature (Table I) above room temperature [26].

Following Tanaka & Ozaki [40,41], we express the generalized electronegativity of metal ions in the metal oxide (χi) as $\chi i = (1 + 2Z)\chi_0$, where χ_0 is the Pauling's electronegativity of the metal element and Z is the valence of metal ions (Table III). In Fig. 7 we plot the onset temperature of the exothermic reaction and the amount of heat released during the AN decomposition in the reactor against χi considering the M^{2+} cations. We observe that there is a correlation between the catalytic effect of the ferrites in AN thermal decomposition and the electronegativity of M^{2+} cations in the sense that, the higher the electronegativity, the higher is the amount of heat released. Excepting MgFO, there is also a correlation for the onset temperature, which decreases with respect to pure AN. The results indicate that those cations with partially filled *d* shells like Co^{2+} ($3d^7$) in CoFO have the highest influence, followed by Cu^{2+} ($3d^9$) in CuFO. For MgFO and ZnFO with noble gas configuration and a completely filled *d* shell, respectively, the effect of these ferrites is less effective. Co ferrite is the most promising catalyst for increased heat release at the lowest temperature.

Summarizing, the effect of nanostructured ferrites on the AN decomposition can be explained as follows. Firstly, NO_3^- and NH_4^+ are formed by the dissociation of molten AN above its melting point. This is followed by a proton transfer from NH_4^+ to NO_3^- to produce HNO_3 and NH_3 in chemical equilibrium. The metal cations are acidic Lewis sites that participate in the removal of ammonia through the adsorption of NH_3 that acts as a Lewis base. Those cations M^{2+} cations with higher electronegativity will be more efficient in removing NH_3, favoring the exothermic oxidation reaction with HNO_3, or its reaction products that intervene mainly in the inner of the liquid phase. This also explains the null effect under open or partially open conditions where endothermic vaporization of HNO_3 and NH_3 dominates the decomposition process.

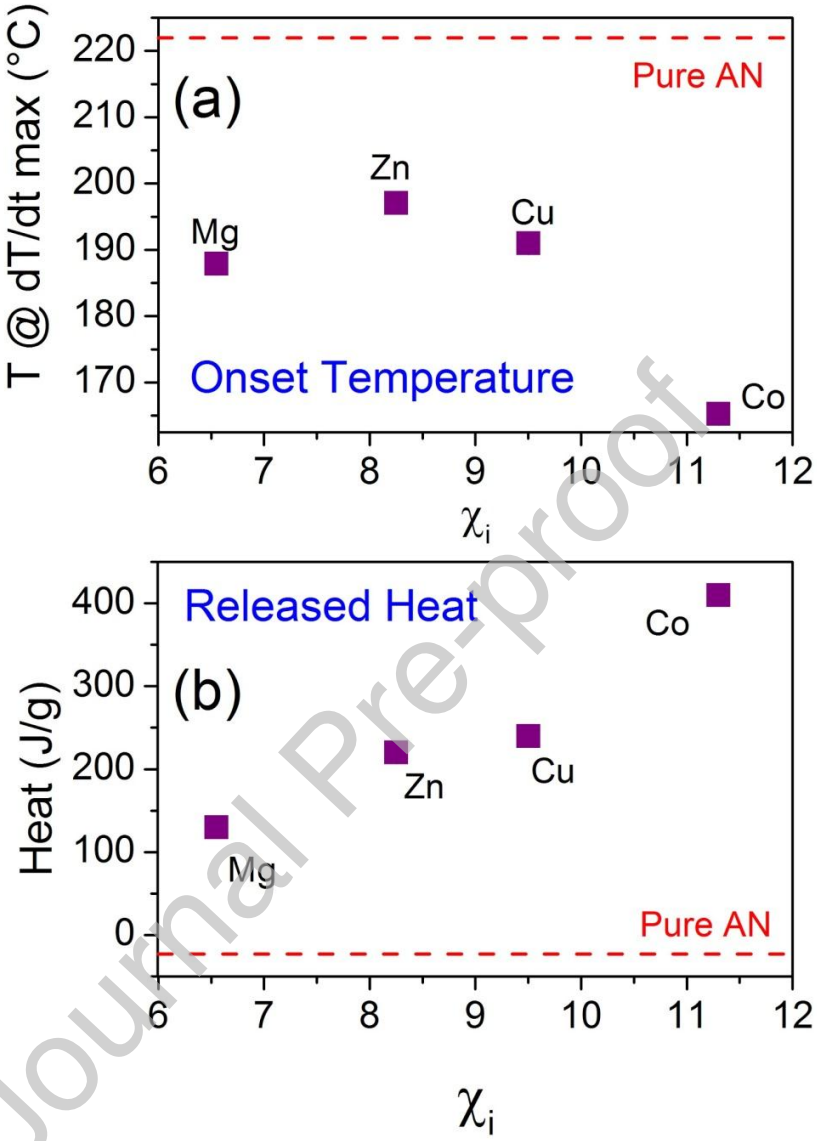

Figure 7: (a) Temperatures at which the maxima (*dT*/*dt* max) are registered in the reactor for AN-ferrite mixtures and (b) Heat released during the decomposition (DSC experiments under sealed condition) as a function of the generalized electronegativity (χ_i). Errors bars are included inside the symbols.

5. Conclusion

Nanostructured ferrites MFe_2O_4 (M= Co, Cu, Mg, Zn) were synthesized via autocombustion method and characterized by several techniques, aiming to employ these compounds to catalyze the decomposition of ammonium nitrate for its use as propellant. The thermal decomposition of ammonium nitrate manifests as an endothermic reaction when the DSC studies were performed in an open pan or in a pan with a lid. Under sealed conditions the pressure level achieved reduces the evaporation process of HNO_3 and NH_3 and AN undergoes an exothermic reaction.

The addition of ferrites affects the AN thermal decomposition under sealed conditions. In such a case, the most remarkable effects of the catalysts were to reduce the onset temperature of the exothermic reaction detected in the reactor and increase the heat released during the decomposition in the DSC experiments. The highest to the lowest shift of the onset temperature was found to be CoFO > MgFO > CuFO > ZnFO. The AN+MFe_2O_4 results indicate that the catalytic effect is more relevant for those ferrites that are composed by M^{2+} cations with the largest electronegativity, which act as Lewis acid sites that participate in the removal of NH_3 or its reaction products. The major effects were observed to occur in AN+CoFO. These findings might encourage the use of mixed ferrites or other semiconductor oxides with metal transition ions adequate to facilitate a good performance on the decomposition of AN for its use as propellant.

Declaration of interests

The authors declare that they have no known competing financial interests or personal relationships that could have appeared to influence the work reported in this paper.

The authors declare the following financial interests/personal relationships which may be considered as potential competing interests.

Acknowledgements

We thank CONICET and UNLP, La Plata, Argentina, for financial support.

5. References

[1] Oommen C, Jain SR, Ammonium nitrate: a promising rocket propellant oxidizer. *J. Hazard Mater* 1999;**67:**253-281. https://doi.org/10.1016/S0304-3894(99)00039-4.

[2] Page JC, Miskimins JL, A Comparison of Hydraulic and Propellant Fracture Propagation in a Shale Gas Reservoir, *J Can Pet Technol* 2009; **48**: 26-30. https://doi.org/10.2118/09-05-26

[3] Hadzik J, Koślik P, Wilk Z, Frodyma A, Habera Ł, Experimental Study on Ammonium Nitrate (V)-based Solid Propellants for Fracturing Wells. *Central European Journal of Energetic Materials*, 2017;**14**: 660-674, DOI 10.22211/cejem/76721

[4 Kumar P, Joshi PC, Kumar R. Thermal decomposition and combustion studies of catalyzed AN/KDN based solid propellants, *Combustion and Flame.* 2016;**166**:316-32, https://doi.org/10.1016/j.combustflame.2016.01.032

[5] Chaturvedi S, Dave PN, Review on thermal decomposition of ammonium nitrate, *J. Energ Mater* 2013;**31:**1-26. https://doi.org/10.1080/07370652.2011.573523.

[6] Trache D, Klapötke TM, Maiz L, Abd-Elghany M, DeLuca LT, Recent advances in new oxidizers for solid rocket propulsion, *Green Chem* 2017;**19**:4711-4736. https://doi.org/10.1039/C7GC01928A.

[7] Jos J, Mathew S, Ammonium nitrate as an eco–friendly oxidizer for composite solid propellants: promises and challenges. *Crit Rev Solid State* 2017;**42**:470-498. https://doi.org/10.1080/10408436.2016.1244642.

[8] Ammonium Nitrate. In: Synthetic Nitrogen Products. Springer, Boston, MA. 2005. https://doi.org/10.1007/0-306-48639-3_10

[9] Iqbal S, Riaz U, Murtaza G, Jamil M, Ahmed M, Hussain A, Abbas Z, Chemical Fertilizers, Formulation, and Their Influence on Soil Health. In *Microbiota and Biofertilizer* 2021; 1-15. Springer, Cham. https://doi.org/10.1007/978-3-030-48771-3_1

[10] Atamanov M, Yelemessova Z, Imangazy A, Kamunur K, Lesbaev B, Mansurov Z, Yue T, Shen R, Yan QL, The catalytic effect of CuO-doped activated carbon on thermal decomposition and combustion of AN/Mg/NC composite. *J. Phys Chem* C 2019; **123**:22941-22948. https://doi.org/10.1021/acs.jpcc.9b05094.

[11] Naya T, Kohga M, Burning characteristics of ammonium nitrate- based composite propellants supplemented with Fe_2O_3, *Propellants Explos Pyrotech* 2013;**38:**547-54. https://doi.org/10.1002/prep.201200159.

[12] Xu ZX, Xu GS, Fu XQ, Wang Q, The mechanism of nano-CuO and $CuFe_2O_4$ catalyzed thermal decomposition of ammonium nitrate. *Nanomater Nanotechno* 2016; **6:**1847980416681699. https://doi.org/10.1177/1847980416681699.

[13] Larionov KB, Mishakov IV, Gromov AA, Zenkov AV, The influence of nanoxide additives on the characteristics of thermal decomposition of ammonium nitrate. *J. Phys. Conf Ser* 2018;**1128**:012065. https://doi.org/10.1088/1742-6596/1128/1/012065.

[14]Vara JA, Dave PN, Chaturvedi S, The catalytic investigation of nanoferrites on the thermal decomposition behavior of AN-based composite solid propellant. *Particul Sci Technol* 2019;**15:**1-9. https://doi.org/10.1080/02726351.2019.1639866.

[15] Vara JA, Dave PN, Metal oxide nanoparticles as catalyst for thermal behavior of AN based composite solid propellant. *Chem Phys Let.* 2019;**730:**600-607. https://doi.org/10.1016/j.cplett.2019.06.048.

[16] Jacobs JP, Maltha A, Reintjes JG, Drimal J, Ponec V, Brongersma HH, The surface of catalytically active spinels, *J. Catal.* 1994;**147:**294-300. https://doi.org/10.1006/jcat.1994.1140.

[17] Albuquerque AS, Tolentino MV, Ardisson JD, Moura FC, de Mendonça R, Macedo WA, Nanostructured ferrites: structural analysis and catalytic activity. *Ceram In.* 2012;**38**:2225-2231. https://doi.org/10.1016/j.ceramint.2011.10.071.

[18] Liu T, Wang L, Yang P, Hu B, Preparation of nanometer $CuFe_2O_4$ by auto-combustion and its catalytic activity on the thermal decomposition of ammonium perchlorate. *Mater. Lett.* 2008;**62:**4056-4058. https://doi.org/10.1016/j.matlet.2008.04.081.

[19] Alizadeh-Gheshlaghi E, Shaabani B, Khodayari A, Azizian-Kalandaragh Y, Rahimi R, Investigation of the catalytic activity of nano-sized CuO, Co_3O_4 and $CuCo_2O_4$ powders on thermal decomposition of ammonium perchlorate. *Powder Technol* 2012;**217:**330-339. https://doi.org/10.1016/j.powtec.2011.10.045.

[20] Hwang C, Wu T, Wan J, Tsai J, Development of a novel combustion synthesis method for synthesizing of ceramic oxide powders. *Mater Sci Eng. B-Adv* 2004;**111:**49-56. https://doi.org/10.1016/j.mseb.2004.03.023.

[21] Skordilis CS, Pomonis PJ, The influence of Mn, Co and Cu cations on the thermal decomposition of NH_4NO_3 in pure form and supported on alumina. *Thermochim Acta* 1993;**216**:137-146. https://doi.org/10.1016/0040-6031(93)80387-P.

[22] Hoffmann J, Kaniewski M, Nieweś D, Hoffmann K, Selected magnesium compounds as possible inhibitors of ammonium nitrate decomposition. *Pol J Chem Technol* 2020;**22**:1-8. https://doi.org/10.2478/pjct-2020-0011.

[23] Smit J, Wijn HP, Ferrites: physical properties of ferri-magnetic oxides in their relation to their technical applications, Eindhoven, The Netherlands: Philips Technical Library; 1959.

[24] Cabrera AF, Rodriguez Torres CE, Marchetti SG, Stewart SJ, Degradation of methylene blue dye under dark and visible light conditions in presence of hybrid composites of nanostructured $MgFe_2O_4$ ferrites and oxygenated organic compounds. *J. Environ Chem Eng* 2020:**8:**104274. https://doi.org/10.1016/j.jece.2020.104274.

[25] Evans BJ, Hafner SS, Mössbauer resonance of Fe^{57} in oxidic spinels containing Cu and Fe. *J Phys Chem Solids* 1968;**29:**1573–1588. https://doi.org/10.1016/0022-3697(68)90100-5.

[26] Stewart SJ, Figueroa SJA, Sturla MB, Scorzelli RB, García F, Requejo FG, Magnetic ZnFe2O4 nanoferrites studied by X-ray magnetic circular dichroism and Mössbauer spectroscopy, *Physica B* 2007;**389:**155-158. https://doi.org/10.1016/j.physb.2006.07.045

[27] Babrauskas V, Leggett D, Thermal decomposition of ammonium nitrate, *Fire Mater* 2020;**44**:250-268. https://doi.org/10.1002/fam.2797.

[28] Harju ME, Solid-state transition mechanisms of ammonium nitrate phases IV, III, and II investigated by simultaneous Raman spectrometry and differential scanning calorimetry, *Appl Spectrosc* 1993;**47:**1926-1930. https://doi.org/10.1366/0003702934066127.

[29] Izato YI, Miyake A, A condensed phase decomposition mechanism for ammonium nitrate. *Sci Technol Energ Mater* 2015;**76**:98-103.

[30] Yang M, Chen X, Wang Y, Yuan B, Niu Y, Zhang Y, Liao R, Zhang Z, Comparative evaluation of thermal decomposition behavior and thermal stability of powdered ammonium nitrate under different atmosphere conditions. *J Hazard. Mater* 2017;**337**:10-19. https://doi.org/10.1016/j.jhazmat.2017.04.063.

[31] Tsyganenko AA, Pozdnyakov DV, Filimonov VN, Infrared study of surface species arising from ammonia adsorption on oxide surfaces. *J Mol Struct* 1975;**29**:299-318. https://doi.org/10.1016/0022-2860(75)85038-1.

[32] Abee MW, Cox DF, NH_3 chemisorption on stoichiometric and oxygen-deficient SnO_2(110) surfaces. *Surf Sci* 2002;**520**:65-77. https://doi.org/10.1016/S0039-6028(02)02247-1.

[33] Apostolescu N, Geiger B, Hizbullah K, Jan MT, Kureti S, Reichert D, Schott F, Weisweiler W, Selective catalytic reduction of nitrogen oxides by ammonia on iron oxide catalysts. *Appl Catal. B* 2006;**62**:104-114. https://doi.org/10.1016/j.apcatb.2005.07.004.

[34] Nalimova SS, Kondrat'ev VM, Study of surface acid-base properties of gas-sensitive metal oxides, *IEEE Conference of Russian Young Researchers in Electrical and Electronic Engineering* (EIConRus) 2020, 987-990. https://doi.org/10.1109/EIConRus49466.2020.9039264.

[35] Bhardwaj A, Kumar A, Sim U, Im HN, Song SJ, Synergistic enhancement in the sensing performance of a mixed-potential NH_3 sensor using SnO_2@$CuFe_2O_4$ sensing electrode. *Sens Actuators B Chem* 2020;**308**:127748. https://doi.org/10.1016/j.snb.2020.127748.

[36] Vargeese AA, Muralidharan K, Kinetics and mechanism of hydrothermally prepared copper oxide nanorod catalyzed decomposition of ammonium nitrate. *Appl Catal A* 2012;**447**:171-177. https://doi.org/10.1016/j.apcata.2012.09.027.

[37] Cannon J, Zhang Y, Catalytic decomposition of potassium chlorate. *J Therm Anal Calorim* 1994;**41**:981-93. https://doi.org/10.1007/bf02547189.

[38] Ramankutty CG, Sugunan S, Surface properties and catalytic activity of ferrospinels of nickel, cobalt and copper, prepared by soft chemical methods. *Appl Catal A* 2001;**218**:39-51. https://doi.org/10.1016/S0926-860X(01)00610-X.

[39] Salcedo Rodríguez KS, Melo Quintero JJ, Medina Chanduví HH, Gil Rebaza AV, Faccio R, Adeagbo WA, Hergert W, Rodriguez Torres CE, Errico LA, Ab-initio approach to the stability and the structural, electronic and magnetic properties of the (001) $ZnFe_2O_4$ surface terminations. *Appl Surf Sci* 2020;**499**:143859. https://doi.org/10.1016/j.apsusc.2019.143859.

[40] Tanaka KI, Ozaki A, Acid-base properties and catalytic activity of solid surfaces. *J. Catal.* 1967;**8**:1-7. https://doi.org/10.1016/0021-9517(67)90274-6.

[41] Ishida T, Takamura R, Takei T, Akita T, Haruta M, Support effects of metal oxides on gold-catalyzed one-pot N-alkylation of amine with alcohol. *Appl Catal A* 2012;**413**:261-6. https://doi.org/10.1016/j.apcata.2011.11.017

Figure Captions

Figure 1: XRD diffractograms of M- ferrites obtained by autocombustion. Miller indices (*hkl*) indicate the spinel characteristic lines

Figure 2: SEM micrographs corresponding to (a) MgFO, (b) CoFO, (c) CuFO and (d) ZnFO ferrites samples.

Figure 3: Thermal treatments for pure ammonium nitrate: (a) Differential scanning calorimetry (DSC) analysis under different conditions, (b) Thermogravimetric analysis (TGA) curves for open and sealed pan conditions, (c) Differential thermogravimetric DTG curves for open and sealed pan conditions (inset: DTG and DSC curves for sealed pan), (d) Temperature of the reactor chamber and (e) change of pressure as a function of time. Insets of (d) and (e) show the corresponding derivatives.

Figure 4: DSC curves for pure AN and AN+MFe_2O_4 mixtures placed in a sealed aluminum pan. The curves were shifted vertically for a better visualization.

Figure 5: (a) Temperature of the reactor chamber and (b) change of pressure (P-P_0) and as a function of time for treatments of pure AN and AN+ferrite mixtures.

Figure 6: Graph showing the temperatures at which the maxima (dT/dt max) and minima (dT/dt min) of the derivatives of $T(t)$ and of the maximum change of pressure $P(t)$ are registered in the reactor for AN and AN+ferrite mixtures (Fig. 3). Error bars are included inside the symbols.

Figure 7: (a) Temperatures at which the maxima (dT/dt max) are registered in the reactor for AN-ferrite mixtures and (b) Heat released during the decomposition (DSC experiments under sealed condition) as a function of the generalized electronegativity (χi). Errors bars are included inside the symbols.

Table Captions

Table I: Average crystallite size (L) and lattice parameter (a) resulting from the XRD data and magnetic ordering temperature (T_C) determined by TGA measurements. The T_C of CoFO was not obtained. Values of reported a and T_C (or the Neel temperature T_N for ZnFO) of cubic ferrites are also included (Refs. [23,25]). (*PDF # 77-0010;✦PDF # 22-1086). E_g is the energy band gap estimated from the UV-Vis spectroscopy data.

Table II: Values corresponding to the DSC and TGA results on pure AN. [a]Refs. [5,7,28]. [*]Temperature range.

Table III: Temperature values of peak (3) and heat released corresponding to the decomposition reaction peak (4) extracted from DSC results of hermetically sealed condition measurements. [*]χ_i is the electronegativity of metal ion in metal oxide supports (Ref. [40]).